Electronic Supplementary Material (ESI) for Nanoscale.
This journal is © The Royal Society of Chemistry 2019

Supplementary Information

Local-ordering PtNiPb ternary nano-pompons as efficient bifunctional oxygen reduction and methanol oxidation catalyst

Na Cheng, Ling Zhang, Hao Jiang, Yingjie Zhou, Shengwei Yu, Liyuan Chen, Haibo Jiang* and Chunzhong Li*

Key Laboratory for Ultrafine Materials of Ministry of Education, Shanghai Engineering Research Center of Hierarchical Nanomaterials, School of Materials Science and Engineering, East China University of Science & Technology, Shanghai 200237, China

*Corresponding author, Tel.: +86-21-64250996, +86-21-64250949

E-mail: jianghaibo@ecust.edu.cn (Prof. H. B. Jiang), czli@ecust.edu.cn (Prof. C. Li)

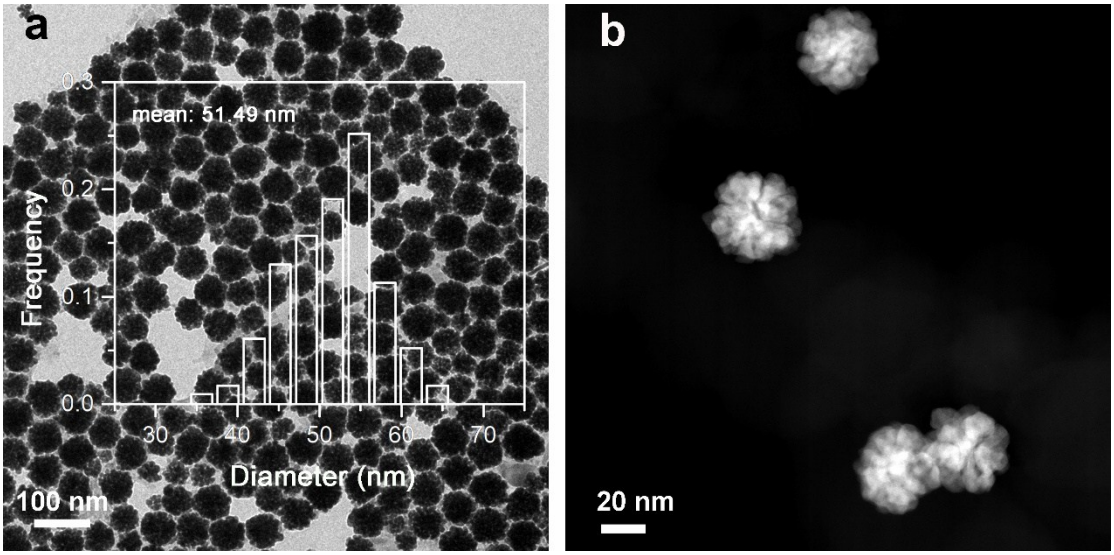

Figure S1. (a) Low-resolution TEM image (inset is the corresponding particle size distribution histogram), and (b) HAADF-STEM image of PtNiPb NPs.

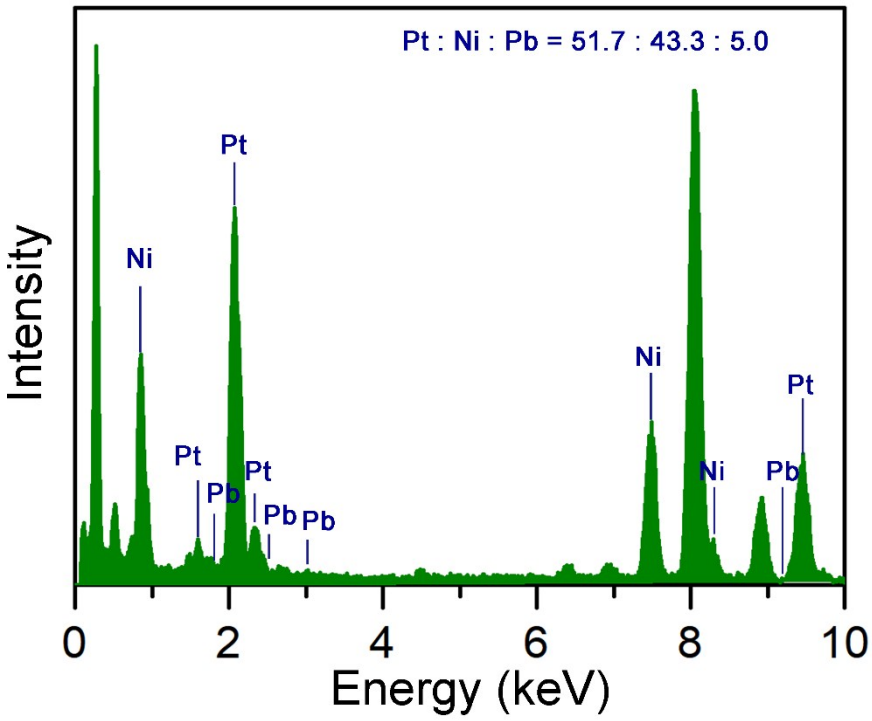

Figure S2. STEM-EDS spectra of PtNiPb NPs.

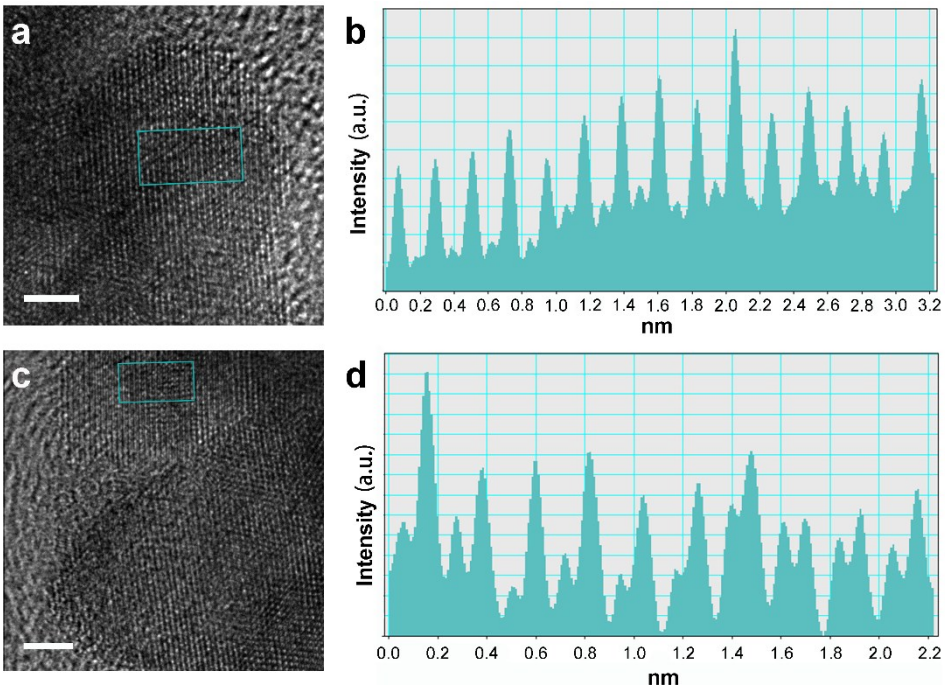

Figure S3. a), c) Additional HRTEM images of local superlattice structure, and b), d) the corresponding measured lattice distances. Scale bar: 2 nm.

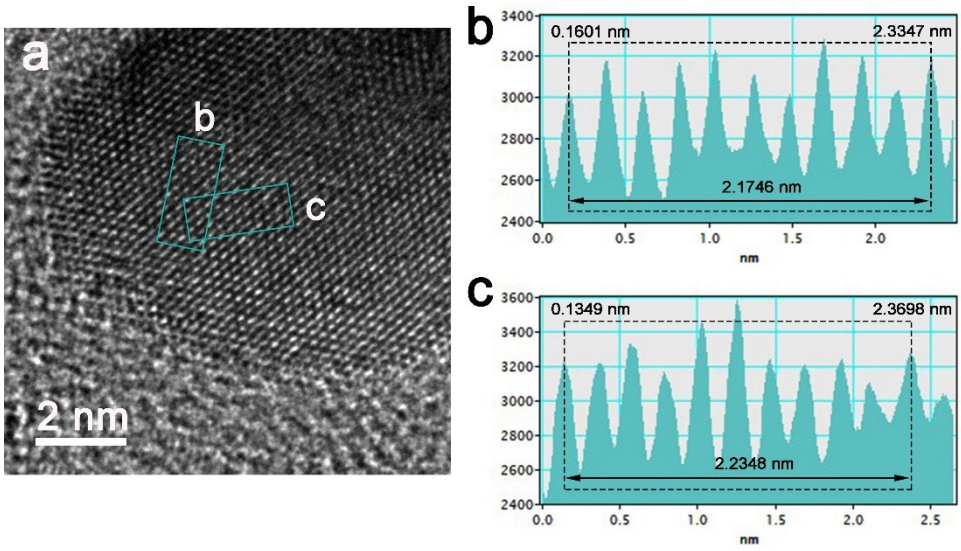

Figure S4. a) HRTEM image of the local-ordering region. b), c) Intensity line profile analysis of the lattice fringes for a). The lattice contraction is 3.9% and 1.3% for b) and c), respectively, compared with Pt(111) (0.2265 nm).

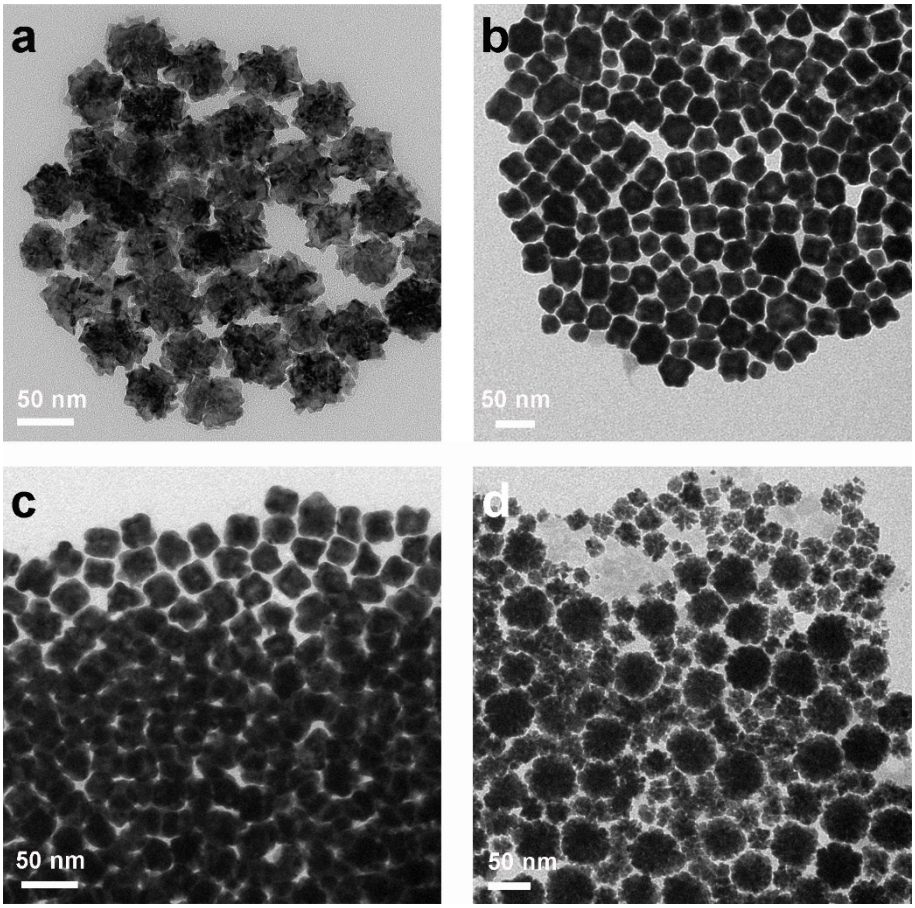

Figure S5. Typical TEM images of the product a) with the same reaction conditions as that of PtNiPb NPs except the absence of $Pb(acac)_2$, b) obtained when three precursors were added at the same time while kept the same heating-cooling process, c) obtained by directly heating the reaction solution that contained three precursors at 180°C for 5 h, and d) obtained when $Pb(acac)_2$ were added without cooling step.

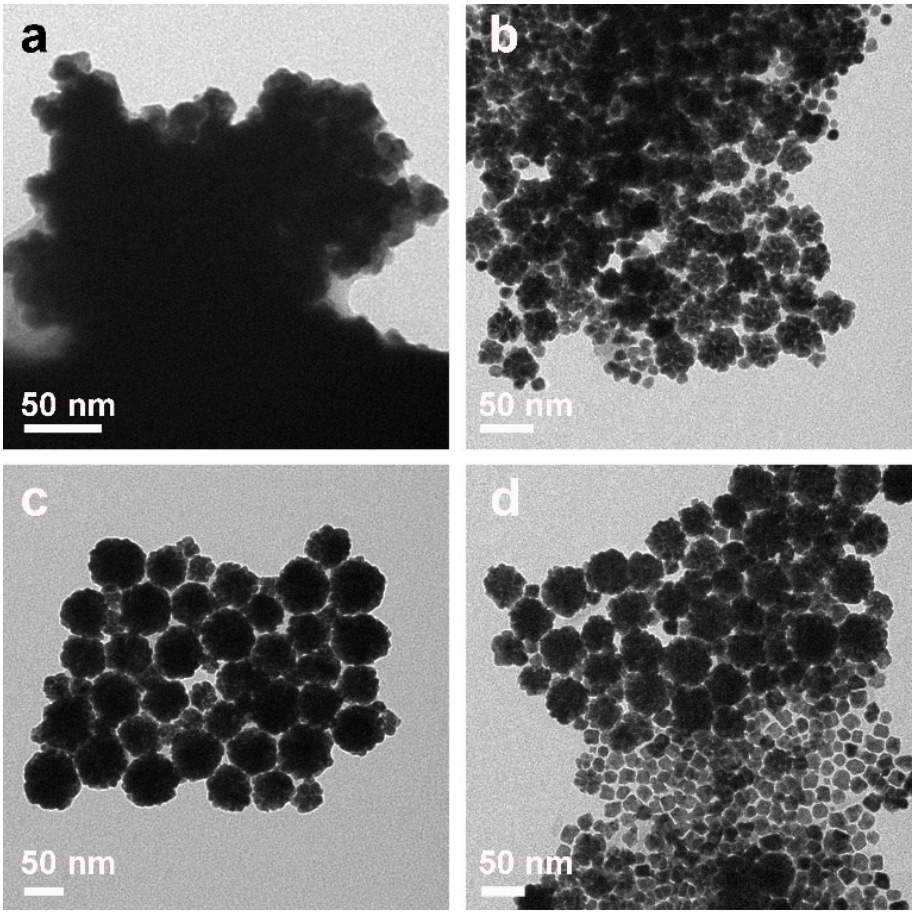

Figure S6. TEM images of the products with the same reaction conditions as those of PtNiPb NPs except the use of (a) no capping agent, (b) CTAC, (C) DTAB and (D) DTAC.

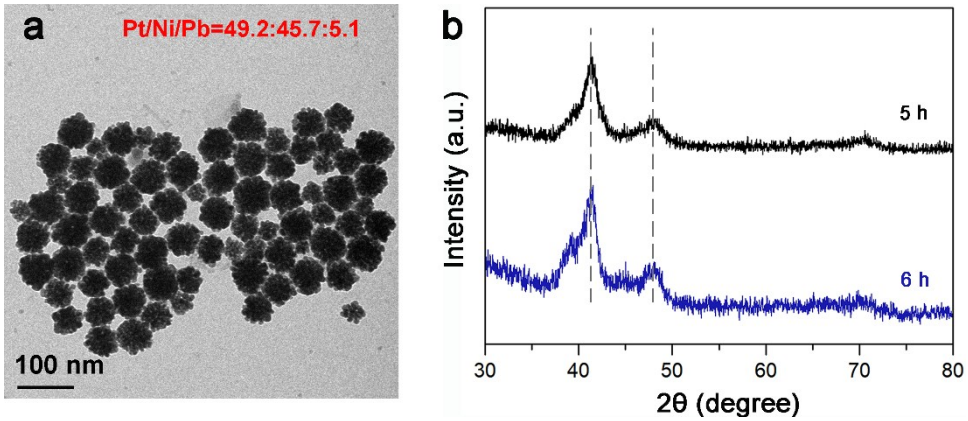

Figure S7. (a) TEM image and elemental composition of the products after the reactant solution was maintained at 180 °C for 6h. (b) Comparison of the XRD patterns of the products at 5h and 6h. The peak positions of the product at 6 h show no shift compared with that at 5 h.

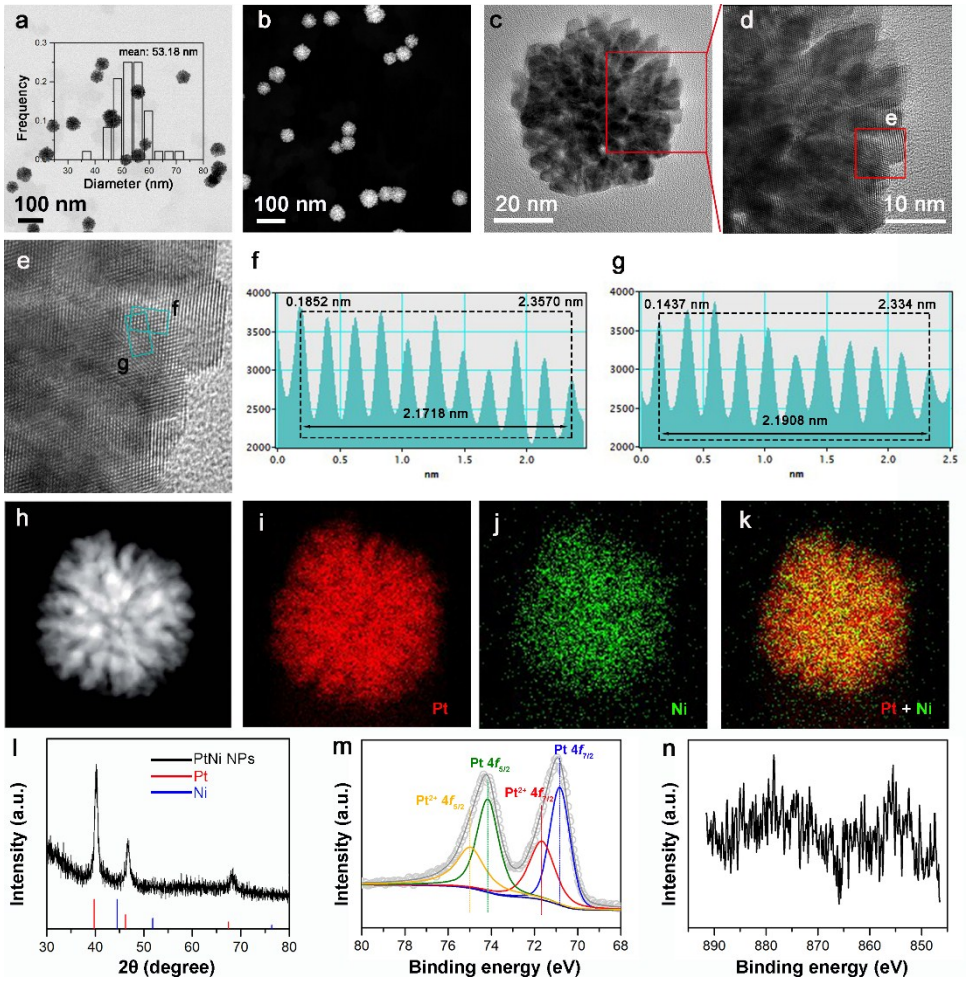

Figure S8. Morphology and structural characterizations of PtNi NPs. a), b) low-resolution TEM image and HAADF-STEM image, respectively. Inset of a) is the particle size distribution histogram. c), d), e) HRTEM images. f), g) Intensity line profile analysis of the lattice fringes for d). h)-k) EDS mapping. l) XRD patterns. m), n) High-resolution XPS spectra of Pt 4f and Ni 2p, respectively.

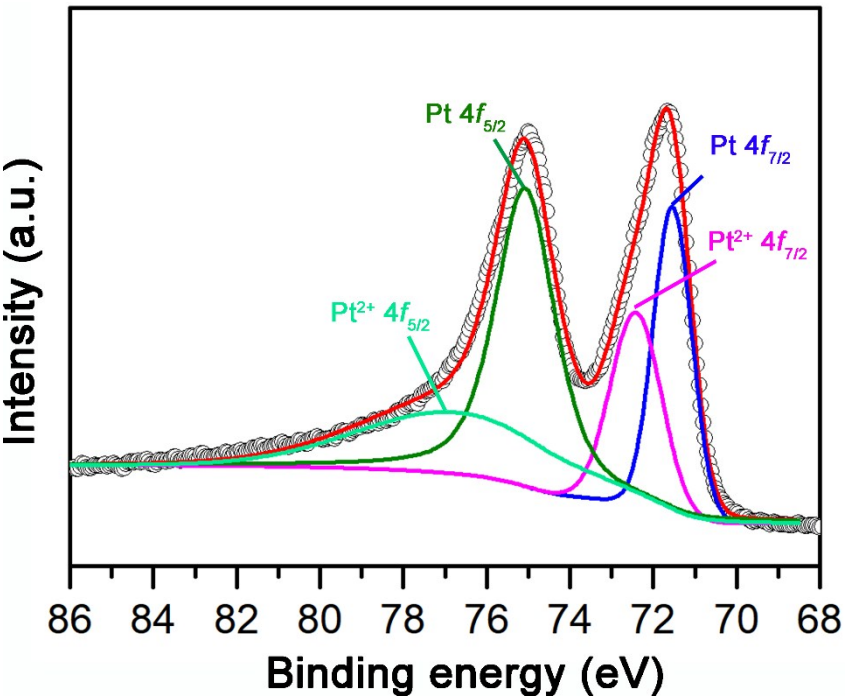

Figure S9. Pt 4f XPS spectra of commercial Pt/C catalyst.

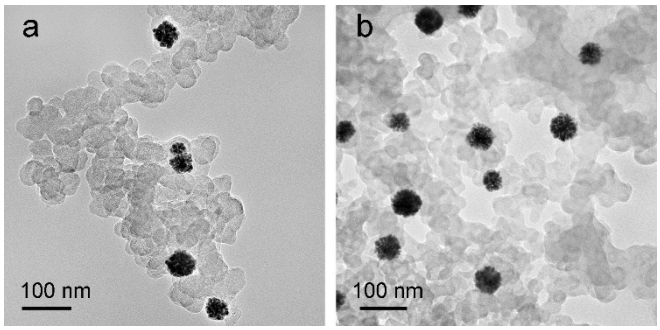

Figure S10. TEM images of carbon supported a) PtNiPb NPs, and b) PtNi NPs catalysts.

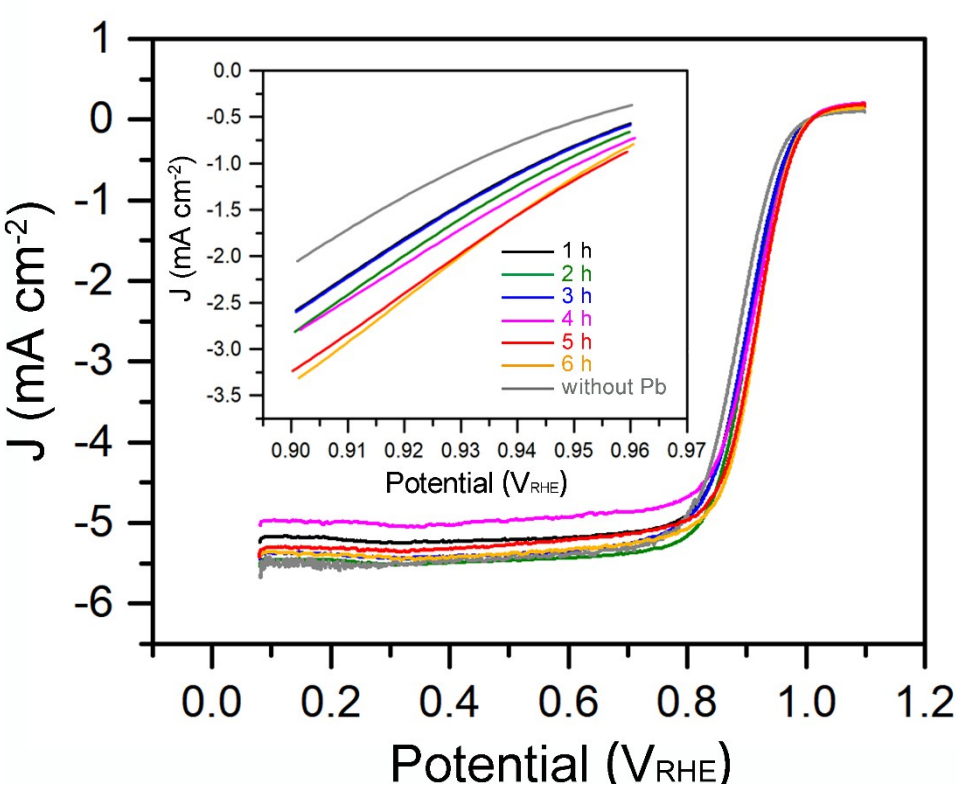

Figure S11. ORR polarization curves of PtNiPb NPs products at different reaction stages.

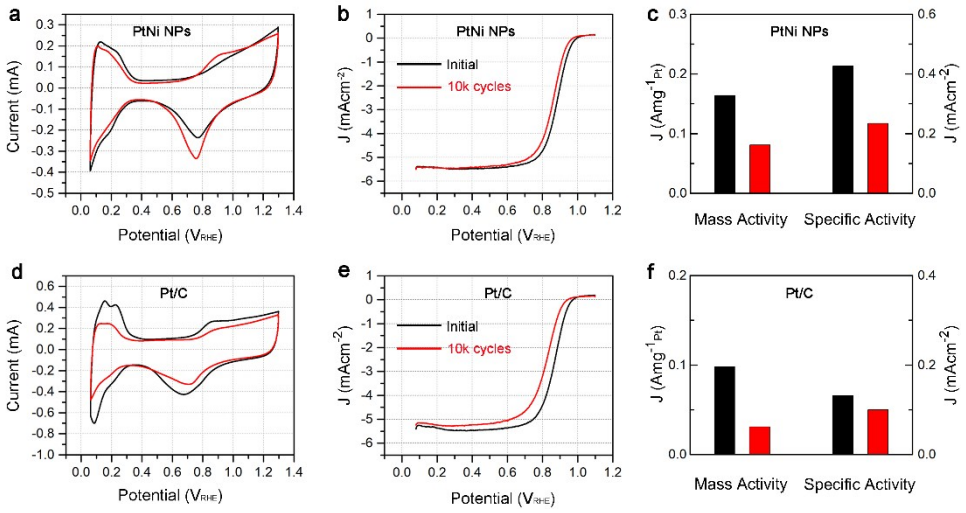

Figure S12. Electrochemical durability towards ORR of PtNi NPs and commercial Pt/C. (a), (d) CVs curves, (b), (e) ORR polarization curves, and (c), (f) the changes in MA and SA after 10 000 potential cycles of (a), (b), (c) PtNi NPs, and (d), (e), (f) commercial Pt/C, respectively.

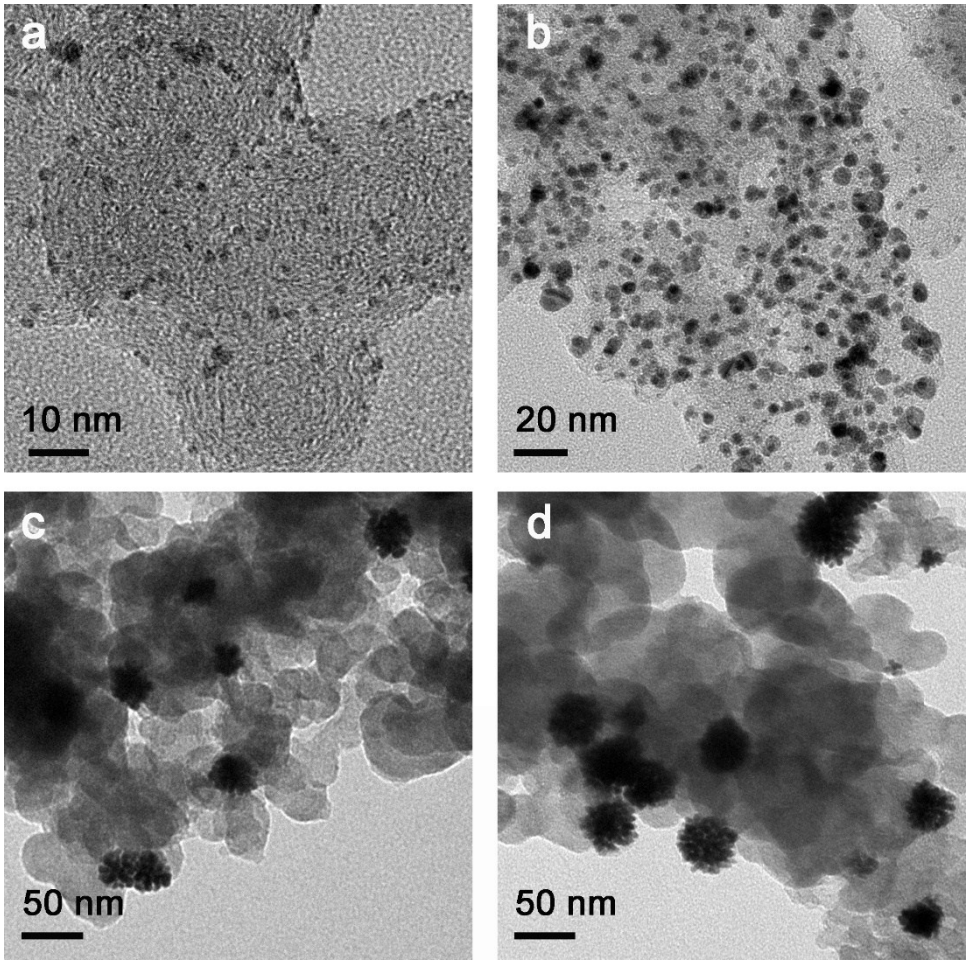

Figure S13. a), b) TEM images of commercial Pt/C before and after 10000 ADTs, respectively. c), d) TEM images of PtNi NPs and PtNiPb NPs after 10000 ADTs, respectively.

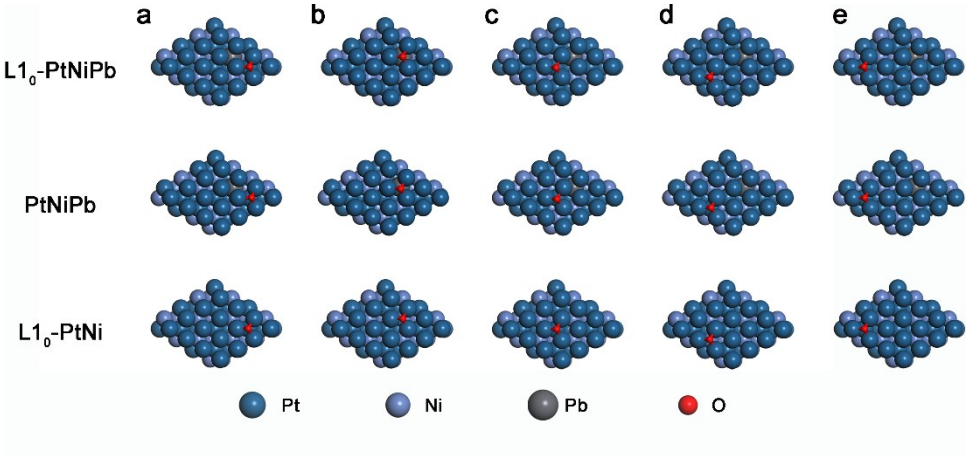

Figure S14. Atomic models for the calculation of E_{ads}(O) at different adsorption sites.

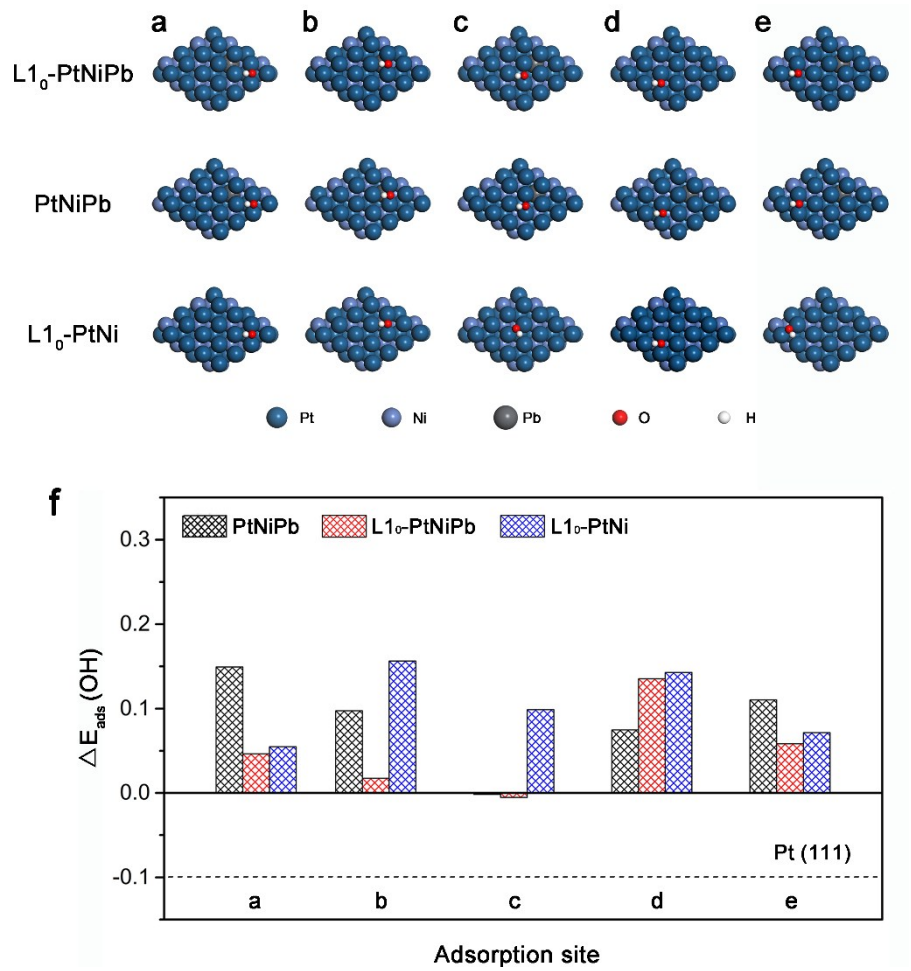

Figure S15. a)-e) Atomic models for the calculation of E_{ads}(OH) at different adsorption sites. f) Comparison of ΔE_{ads}(OH) on the (111) surface of L1$_0$-PtNiPb, PtNiPb, and L1$_0$-PtNi. The optimal E_{ads}(OH) value is 0.1 eV weaker than that of Pt(111). the overall trend of ΔE_{ads}(OH) is consistent with that of ΔE_{ads}(O), where the superlattice structure and the embedded Pb atom can increase the adsorption energy of OH. For the adsorption sites b and c of L1$_0$-PtNiPb, the ΔE_{ads}(OH) values are 0.017 and -0.005 eV, respectively, very close to the optimal energy. The weaker E_{ads}(OH) of the adsorption site d in L1$_0$-PtNiPb and L1$_0$-PtNi compared with PtNiPb can be attributed to the strong coupling between surface Pt and subsurface Ni.

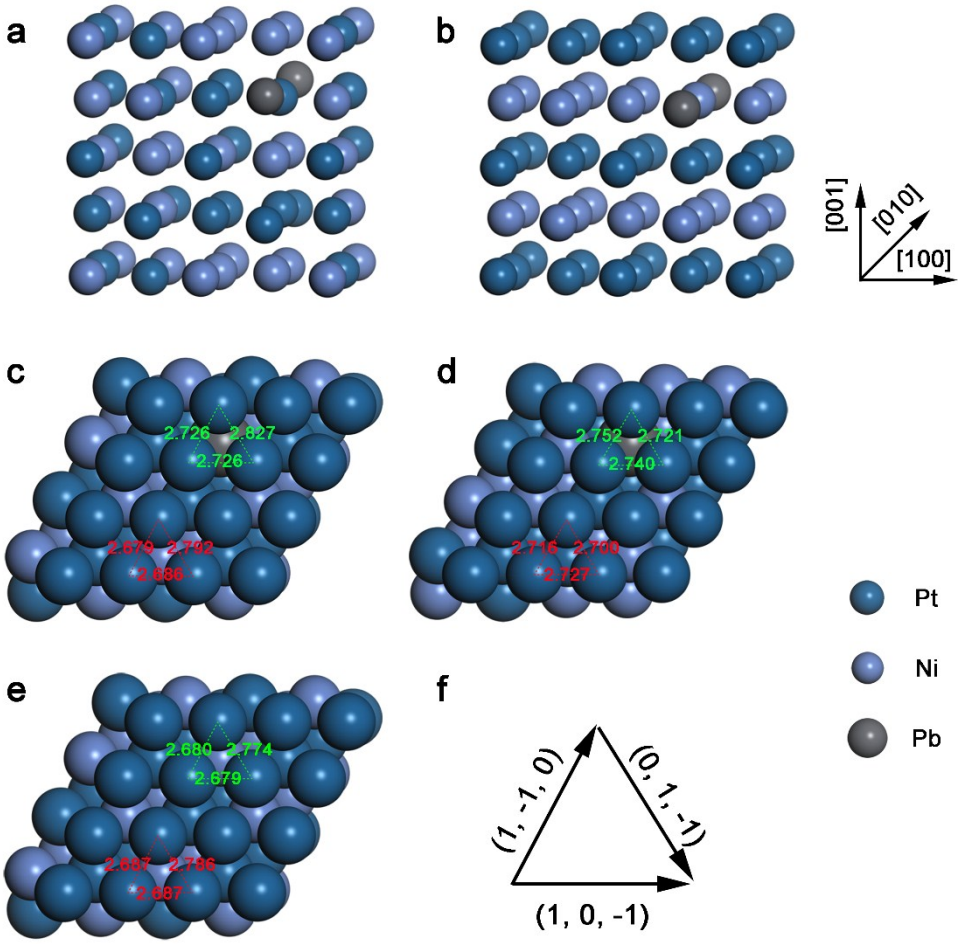

Figure S16. a), b) The periodic supercells of PtNiPb and $L1_0$-PtNiPb, respectively. Comparison of atomic distances on (111) surfaces of c) $L1_0$-PtNiPb, d) PtNiPb, and e) $L1_0$-PtNi along the vectors shown in f). It is shown that the chemically ordered $L1_0$ structure can slightly release the strong lattice compression along (0, 1, -1) direction, and the doping of Pb can further moderate the surface strain.

Table S1. XPS data of Pt/C, PtNi NPs and PtNiPb NPs.

		Pt/C	PtNi NPs	PtNiPb NPs
Pt^0/Pt^{2+}		1.54	1.39	1.86
Peak Position (eV)	$Pt\ 4f_{7/2}$	71.65	70.82	71.01
	$Pt\ 4f_{5/2}$	75.00	74.16	74.34

Table S2. ECSAs, half-wave potentials, and ORR activities of different catalysts.

	ECSA ($m^2\ g^{-1}_{pt}$)	Half-wave potential (V_{RHE})	SA ($mA\ cm^{-2}$)	MA ($A\ mg^{-1}_{Pt}$)
PtNiPb NPs	48.32	0.917	0.976	0.449
PtNi NPs	38.42	0.883	0.427	0.164
Pt/C	73.74	0.868	0.132	0.098

Table S3. ORR durability of PtNiPb NPs, PtNi NPs, and Pt/C.

		ECSA (m^2/g_{pt})	SA ($mAcm^{-2}$)	MA (Amg^{-1}_{Pt})	loss in MA
PtNiPb NPs	initial	48.32	0.976	0.449	
	10k	38.98	0.827	0.322	28.3%
PtNi NPs	initial	38.42	0.427	0.164	
	10k	34.68	0.234	0.081	50.6%
Pt/C	initial	73.74	0.132	0.098	
	10k	31.08	0.100	0.031	68.4%

Table S4. Calculated d-band center of representative atoms.

		d-band center
$L1_0$-PtNiPb	**A1**	-2.82
	A2	-2.74
$L1_0$-PtNi	**A1**	-2.84
	A2	-2.82
PtNiPb	**A1**	-2.94
	A2	-2.78
Pt (111)	**A1**	-2.55
	A2	-2.55

Table S5. Crystalline lattice constants and lattice contraction (%) of PtNiPb and $L1_0$-PtNiPb based on DFT calculations.

	$a_{[100]}/a_{Pt}$	**lattice contraction (%)**	$a_{[010]}/a_{Pt}$	**lattice contraction (%)**	$a_{[001]}/a_{Pt}$	**lattice contraction (%)**
PtNiPb	0.966	3.4	0.949	5.1	0.968	3.2
$L1_0$-PtNiPb	0.987	1.3	0.987	1.3	0.922	7.8

a_{Pt} is the lattice constant of fcc-Pt. $a_{[100]}$, $a_{[010]}$, $a_{[001]}$ are the calculated interplanar distances along [100], [010] and [001] directions of PtNiPb and $L1_0$-PtNiPb.

Table S6. Surface strain (ε, in %) on (111) surfaces from DFT Calculations.

	Nonadjacent to Pb			**Adjacent to Pb**		
	PtNiPb	**$L1_0$-PtNi**	**$L1_0$-PtNiPb**	**PtNiPb**	**$L1_0$-PtNi**	**$L1_0$-PtNiPb**
$\varepsilon_{(0, 1, -1)}$	4.3	1.2	1.3	3.5	1.6	-0.2
$\varepsilon_{(1, -1, 0)}$	3.7	4.2	4.6	2.4	5.0	3.3
$\varepsilon_{(1, 0, -1)}$	3.9	4.5	4.5	2.8	5.0	3.3

Compressive strain is calculated by $\varepsilon_i = (a_{Pt} - a_i)/a_{Pt}$, where i indicates directions along (0, 1, -1), (1, -1, 0), and (1, 0, -1) vectors as shown in Figure S16.

Table S7. MOR performance of different catalysts.

	I_f/I_b	SA ($mAcm^{-2}$)	MA (Amg^{-1}_{Pt})
PtNiPb NPs	1.25	2.40	1.16
PtNi NPs	0.85	1.21	0.46
Pt/C	0.93	0.31	0.27